Title: Raman spectroscopy for the preoperative diagnosis of thyroid cancer and its subtypes: An in vitro proof-of-concept study.

Authors: O'Dea D, Bongiovanni M, Sykiotis GP, Ziros PG, Meade AD, Lyng FM, Malkin A

Journal: Cytopathology : official journal of the British Society for Clinical Cytology

Year: 2019 Jan

Issue: 30

Volume: 1

Pages: 51-60

DOI: 10.1111/cyt.12636

Raman spectroscopy for the preoperative diagnosis of thyroid cancer and its subtypes: an *in vitro* proof-of-concept study

Declan O'Dea[1,2*], Massimo Bongiovanni[3*], Gerasimos P. Sykiotis[4], Panos G. Ziros[4], Aidan D. Meade[2,5], Fiona M. Lyng[2,5#] and Alison Malkin[1#]

[1]School of Biological Sciences, Dublin Institute of Technology
[2]DIT Centre for Radiation and Environment Science, Focas Research Institute, DIT
[3]Institut of Pathology, Lausanne University Hospital, Lausanne, Switzerland
[4]Service of Endocrinology, Diabetology and Metabolism, Lausanne University Hospital, Lausanne, Switzerland
[5]School of Physics & Clinical & Optometric Sciences, Dublin Institute of Technology
* Joint first authors
# Joint senior authors

Correspondence should be addressed to Declan O'Dea, FOCAS Institute, DIT Kevin St, Dublin 8, Ireland. E-mail address: declan.odea@mydit.ie

Abstract

Objective: In 2016 there were an estimated 56,870 new cases of thyroid cancer (TC) in the United States. Fine needle aspiration cytology (FNAC) is the most safe, accurate and cost-effective method for the initial investigation of thyroid nodules. FNAC is limited by the inability to accurately diagnose malignancy in follicular-patterned lesions, and as a result 20% to 30% of cases under investigation for TC are classified as cytologically indeterminate, illustrating a problem with current FNAC procedure. Raman spectroscopy has shown promising results for the detection of many cancers however to date there has been no report on the performance of Raman spectroscopy on thyroid cytological samples. The aim of this study was to examine whether Raman spectroscopy could be used to correctly classify cell lines representing benign thyroid cells and various subtypes of TC.

Methods: A benign thyroid cell line and seven TC cell lines were prepared as ThinPrep® cytology slides and analysed with Raman spectroscopy. Principal components analysis (PCA) and linear discriminant analysis (LDA) were implemented to develop effective diagnostic algorithms for classification of Raman spectra of different TC subtypes.

Results: The spectral differences separating benign and TC cell lines were assigned to differences in the composition of nucleic acids, lipids, carbohydrates and protein in the benign and cancer cells. Good sensitivities (74 - 85%), specificities (65 - 93%) and diagnostic accuracies (71 – 88%) were achieved for the identification of TC.

Conclusion: These findings suggest that Raman spectroscopy has potential for preoperative TC diagnosis on FNAC samples.

Acknowledgements: The authors acknowledge funding from the Fiosraigh Scholarship Dean of Graduate Research School Award. GPS is supported by a Leenaards Foundation Fellowship for Academic Promotion in Clinical Medicine and by Swiss National Science Foundation grant 31003A_153062. The work benefited from COST Action BM1401 (Raman4clinics), supported by European Cooperation in Science and Technology.

Conflict of interest: The authors declare no conflict of interest.

Key words: Raman spectroscopy, thyroid nodule, thyroid neoplasms, cell lines

Introduction

In 2016 there were an estimated 56,870 new cases of thyroid cancer (TC) in the United States[1]. Women account for approximately 75% of these cases, exhibiting a substantially higher rate of incidence of the disease compared to men, but similar mortality. TC incidence has been steadily increasing in recent decades, as reported in the TC epidemiology studies[2,3]. Although improved diagnostic methods, notably ultrasound (US) examination, are the likely reason for the global increase in incidence (especially of smaller nodules), recent studies show that the incidence of aggressive forms associated with higher mortality is also increasing[4].

Of the wide array of malignancies that are characterised as TC, papillary thyroid carcinoma (PTC) is the most common, accounting for approximately 80% of cases. Other histological types include follicular thyroid carcinoma (FTC), Hürthle cell carcinoma, poorly differentiated carcinoma, medullary thyroid carcinoma (MTC), and undifferentiated or anaplastic carcinoma (UTC or ATC, respectively). PTC and FTC emanate from thyroid follicular epithelial cells and are commonly referred to as well differentiated thyroid carcinomas (DTC) [5,6]. MTCs are derived from neuroendocrine cells and represent approximately 5 to 10% of TC[7].

The most common manifestation of TC is as a thyroid nodule. Thyroid nodules are common in the general population, with a prevalence of 2-7% when detected by palpation and 50% when searched for using US examination [5,8]. Despite thyroid nodules having a high incidence rate, approximately 60%-80% are classified as benign, with only 3.5% - 10% presenting as malignancies. Fine needle aspiration cytology (FNAC) is the most accurate and cost-effective method for the initial management of thyroid nodules, and its accuracy is higher when it is conducted under US guidance. FNAC is limited by the inability to accurately diagnose malignancy in follicular-patterned lesions, and as a result more than 20% of cases under investigation for TC are classified as cytologically "indeterminate" [9–12]. The indeterminate category often requires surgical resection to definitively exclude malignancy; however, since approximately 70% of these lesions are finally shown to be benign, surgery is an unnecessary procedure for the vast majority of cases [13,14].

In an attempt to overcome limitations of cytology in the detection of cancer, optical spectroscopic techniques have been investigated as adjunct or alternative approaches[15]. Optical spectroscopic methods use the interaction of light with matter to provide a detailed description of the molecular composition of biological tissue, and so these techniques can be employed to detect biochemical profiles associated with health or disease.

Raman spectroscopy is a form of vibrational spectroscopy based on inelastic scattering. Raman spectra are obtained by irradiating a sample with monochromatic laser light, which interacts with molecules within the sample and induces molecular vibrations. The change in energy between the

incident and inelastically scattered light is called the Raman shift. The Raman spectrum is a plot of the intensity of the scattered light versus the change in energy, given in wavenumbers, cm^{-1}[16–18]. The spectrum produced by the probed molecular vibrations represents a detailed biochemical fingerprint of the cellular components.

Raman spectroscopy has shown promising results for the detection of multiple cancers including cervical, gastrointestinal, breast, brain, and lung cancer[19–22]. The application of Raman spectroscopy for TC diagnosis has also been investigated in studies utilizing cell lines[23,24,25], and tissue sections[26–32]. Harris *et al.*[23] applied Raman spectroscopy to two thyroid cell lines, one cancer cell line (8505C, representing UTC) and one benign cell line (Nthy-ori 3-1), to analyse the cellular differences between benign and malignant cells. Distinct differences in the nucleic acid content of the cancer cells were revealed, and, using neural network analysis a diagnostic sensitivity of 95% was achieved for discrimination of the cancer cell line. Building on Harris' work, Lones *et al.*[24] applied Raman spectroscopy to analyse one benign thyroid cell line and four TC cell lines representing PTC, FTC, MTC and UTC. Alterations in either the molecular conformation or concentration of DNA/RNA, amide I and aromatic amino acids were found to be indicative of cancer. The authors reported good discrimination of the benign cell line from MTC and UTC, and a lower discrimination between cell lines with the same cell of origin, namely benign versus DTC cell lines.

Recent studies have also investigated the feasibility of applying Raman spectroscopy to thyroid tissue samples to detect cancer. These studies used multivariate statistical analysis of Raman spectra to achieve high diagnostic sensitivities and specificities for discrimination between healthy thyroid tissue and TC, and follicular patterned thyroid[27–30].

Application of Raman spectroscopy to thyroid FNAC has not yet been reported. As a first step, the present proof-of-concept study builds on the aforementioned studies by investigating the application of Raman spectroscopy to a benign thyroid cell line and a large number of TC cell lines prepared as ThinPrep® cytology slides, representing FNAC cytological specimens.

Materials and Methods

Cell cultures

Cell lines used were representative of benign thyroid cells and four subtypes of TC: one benign follicular epithelial cell line (NThy-ori 3-1), two PTC cell lines (K1 and TPC1), one FTC cell line (XTC1), two UTC cell lines (8505C and C643) and two MTC lines (CRL-1803TT and MZCRC1). The Nthy-ori 3-1

cell line [catalog no. 90011609, lot no. 13B007, passage no. 16 (p16)] was purchased from Sigma and used at p18. The TT cell line was obtained from the American Type Culture Collection (ATCC CRL1803 TT, lot no. 58785858, no passage information) and was used at p3. All other cell lines (K1, used at p9; TPC1, used at p29; XTC1, used at p17; 8505C used at p21; C643, used at p31; MZCRC1, used at p14 were kindly provided by Prof. Paula Soares (Institute of Molecular Pathology and Immunology of the University of Porto, Portugal). All cell lines were maintained in standard culture conditions at 37°C in a humidified incubator under 5% carbon dioxide. RPMI-1640 with 10% fetal bovine serum (FBS) and 1% Pen-Strep was the medium for most cell lines, with the following exceptions: K1 cells were cultured in DMEM/F12 medium supplemented with 10% FBS; CRL1803TT cells were cultured in F-12K Nutrient Mixture Kaighn's Modification with 10% FBS; MZCRC1 cells were cultured in DMEM with 15% FBS. All culture media were from Invitrogen. Slides for Raman analysis were prepared using a ThinPrep® processor and air dried without final staining.

Raman Measurement

Raman spectra were acquired using a HORIBA Jobin Yvon XploRA^{TM} system (Villeneuve d'Ascq, France) which consists of an Olympus microscope BX41 supplied with a x100 objective (MPlanN, Olympus, NA = 0.9). A 532 nm diode laser source was utilised during the study and was set at 100% power, which gave 8 mW at the objective. The confocal hole was set at 100 µm and coupled to a slit of aperture 100 µm. The system was calibrated to the 520 cm^{-1} spectral line of Silicon and the 1200 lines per mm grating was used. Backscattered light was detected using an air-cooled CCD detector (Andor, 1024 x 256 pixels). The software implemented to manage the spectrometer was Labspec V5.0.

Thirty cells were recorded from each slide. For each cell, a single spectrum was recorded from the cell nucleus, corresponding to the average of two accumulations of 30 seconds. Spectra were also recorded from 30 vacant locations on a ThinPrep® glass slide with identical exposure time in order to obtain representative background glass spectra.

The signal to noise ratio (SNR) was calculated by dividing the difference between the peak signal at 1665 cm^{-1} and the baseline intensity (smooth region after 400 cm^{-1}) by the standard deviation of the peak signal, as described by Desroches *et al*[33]. The mean SNR of all of the spectra included was 102 dB, which was calculated from a range of 77 - 159 dB.

Data pre-processing and analysis

All spectral data analysis was conducted using R software. Pre-processing involved smoothing (Savitzy Golay k=5, w=15), a fifth-order polynomial baseline correction and vector normalisation. Outliers were removed using a Grubbs filter. A non-negatively constrained least squares (NNLS) method was used to remove interfering signals from the glass substrate[34,35]. As described by Ibrahim *et al.*[31], spectra from cellular components, such as nucleic acids, proteins, lipids etc, and the independently recorded glass spectra were used to fit the sample spectra and remove the glass contribution. The data was analysed using Principal Component Analysis (PCA), an unsupervised method which reduces the dimensionality of the data and retains the data which are of greatest importance, known as principal components (PC)[36]. Linear discriminant analysis (LDA), which maximises the separation between different classes and minimises within-class variance, was used together with PCA to develop classification model. When implemented with PCA, LDA uses the PC scores to develop the classification model [36–38]. The first PCs that explained approximately 95% of the variance within the data were used in the PC-LDA classification models.

Results

Mean spectral analysis

Figure 1 depicts the mean benign thyrocyte cell line (Nthy-ori3-1) spectrum and the biological components corresponding to each spectral region. The standard deviation shows that there was minimal variation between the spectra from individual cells and this was also the case for all cell lines. The features in the TC cell line spectra that differ from the benign cell line are demonstrated by the difference spectra in Figures 2-4.

The significant Raman peaks and their corresponding biological components are shown in Table 1. Spectral differences between the benign thyroid cell line and the TC cell lines corresponded to peaks relative to lipids and proteins (524, 820, 1225, 1278, 1310, 1343, 1402, 1435, 1453, 1570, 1661, 1677 cm^{-1}), carbohydrates (477, 941, 1343 cm^{-1}), phosphates (1190 cm^{-1}) and nucleic acids (780, 1330 cm^{-1}), as shown in Figures 2-4. The difference spectra of the FTC and PTC cell lines had similar profiles, with significant peaks at 1225, 1435, 1456 and 1690 cm^{-1} differentiating them from the benign cell line (Figure 2). For the UTC cell lines, consistent spectral differences were observed at 780, 1343, 1190, 1280, 1450 cm^{-1} (Figure 3). Compared to the benign cell line, the MTC cell lines showed consistent spectral differences at 780, 1450, 1570, 1645, and 1673 cm^{-1} (Figure 4).

Linear Discriminant Analysis

In order to evaluate the efficacy of Raman spectroscopy to accurately classify the benign and TC cell lines, PC-LDA classification models were developed using the principal components from PCA of the benign thyroid cell line and each of the TC cell lines. Table 2 shows the results of seven separate PC-LDA models used to classify the benign thyroid cells and each of the TC cell lines. The performance of each two way classification is shown using the sensitivity, specificity and diagnostic accuracy of each model. Diagnostic accuracy is used to describe the proportion of correctly classified spectra (true positive + true negative) among all the classified spectra (true positive + true negative + false positive + false negative)[39]. The first 5 PCs in each case were used to develop the PC-LDA classifiers. PC-LDA classification of Nthy-ori 3-1 (benign) vs. PTC, FTC and MTC cell lines yielded sensitivities of ≥90%, specificities of ≥80% and accuracies of ≥89%. Lower performance was observed for the models discriminating the benign cell line from the UTC cell lines with sensitivity, specificity, and diagnostic accuracy of 77%, 73% and 75% for 8505C, and 87%, 77%, 82% for C643, respectively.

To evaluate the ability of PC-LDA to discriminate benign cells from TC subtypes, cell lines were grouped by their TC subtype. To produce an unbiased classifier, representative spectra from each cell line were selected at random and combined by TC subtype, matching the number of spectra used for the benign cell line. As XTC1 was the only cell line representing FTC, all spectra from this cell line were used, matching the number of spectra used for the benign cell line. Table 3 shows the results achieved for discriminating the benign cell line from the TC cell lines grouped by subtype. Separate two-way classification models using 5 PCs each were developed to discriminate the benign cells from each TC subtype. The MTC and PTC subtypes were discriminated from the benign cell line with diagnostic accuracies of at least 82%. The UTC subtype was classified at a lower accuracy of 71%. Due to similarities in their cellular biochemistry observed in this study, the well differentiated PTC and FTC subtypes were grouped together for analysis, yielding a diagnostic accuracy of 74%.

Table 4 shows the results of the two-way PC-LDA classification models used for the discrimination of the PTC and UTC cell lines, each was developed using 4 PCs. Each two-way classification model yielded sensitivities, specificities and diagnostic accuracies above 92% for each cell line classification. Grouped together, the PTC and UTC subtypes were discriminated with a diagnostic accuracy of 81%.

Table 5 shows the results for the PC-LDA classification of MTC cell lines versus the PTC cell lines. Each classification is the result of separate two-way models using 4 PCs each. The models yielded specificities and diagnostic accuracies ≥93% for each cell line classification, and a diagnostic accuracy of 86% for the two-way discrimination of the MTC and PTC subtypes.

Table 6 shows the performance of separate two-way PC-LDA models in discriminating FTC cell lines from PTC, MTC and UTC cell lines. Discrimination of the follicular XTC1 cell line from the PTC cell lines was achieved using 4 PCs in each PC-LDA model. Diagnostic accuracies of 87% and 85% were

obtained for the K1 and TPC1 cell lines respectively. The FTC cell line was discriminated from the UTC cell lines with diagnostic accuracies above 94%, and from the MTC cell lines with 100% accuracy, each model using 4 PCs. When cell lines were grouped by subtype, FTC was distinguished from MTC with an accuracy of 99% (using 4 PCs), from UTC with a diagnostic accuracy of 89% (using 3 PCs), and from PTC with 79% accuracy (using 5 PCs).

Table 7 summarises the results achieved for separate two-way classifications of the MTC and UTC cell lines. The MTC cell lines were discriminated from the UTC cell lines with diagnostic accuracies ≥97% using 3 PCs in each model, and when grouped together, the MTC cell lines were discriminated from the UTC cell lines with an accuracy of 84% using 4 PCs.

Table 8 demonstrates the performance of a five-way classification model developed using the benign cell spectra and spectra from all the TC subtypes. Representative spectra from each cell line were selected at random and combined into TC subtypes as previously described. The model yielded diagnostic sensitivities from 57-100%, specificities ≥91%, and an overall diagnostic accuracy of 78% using 5 PCs. Figure 5 depicts the scatter plot of the linear discriminant scores of the benign spectra and spectra from each TC subtype. The FTC spectra and the PTC spectra form two close clusters using the first two discriminant functions, which can be discriminated from the benign spectra with some overlap. The MTC spectra form a cluster along the first discriminant function which is distinct from the benign spectra. The UTC subtype clusters adjacent to the benign spectra along the first discriminant function, although using only the first two discriminant functions to plot the scatter plot of the linear discriminant scores, the UTC and benign spectra overlap.

Table 9 shows the performance of the PC-LDA model in discriminating the benign cell line from all of the TC subtypes combined into one group. As before, in order to produce an unbiased classifier, representative spectra from each TC subtype were selected at random and combined into one TC group, giving a total number of TC spectra that was similar to the number of benign spectra. The first 5 PCs were used to develop the two-way PC-LDA model which produced a sensitivity of 74%, specificity of 87%, and overall accuracy of 81% for discriminating benign spectra from the TC spectra.

Discussion

Raman microspectroscopy was performed in this study to obtain a biomolecular characterisation of eight thyroid cell lines. Spectral differences were consistently observed between the benign and TC cell lines with the strongest signals occurring at ~470, ~780, 855, 941, ~1230, 1278, 1343, 1402,

1436, 1456, 1571, 1650, 1690 and 1677 cm^{-1}, representing significant differences in the molecular composition of carbohydrates, nucleic acids, lipids, protein structures and amides, as mapped by Movasaghi *et al*.[40], across the benign and TC cell lines. These peaks differentiating benign thyroid cells and TC cells are in accordance with several of the characteristic TC peaks identified in previous studies using tissue samples and cell lines[23,24,31]. The consistent spectral differences between the benign and TC cell lines observed in our study may be reflective of the malignant transformation that occurs due to the carcinogenic progression of TC[40,41]. These Raman peaks represent the vibrational modes of biomolecules that are altered in quantity or conformation in the malignant cells.

The difference spectrum between the benign cell line and the FTC cell line (XTC1), shows identical strong bands to the difference spectra between the benign cell line and the PTC cell lines. The similar profiles of the difference spectra reveal a comparable biochemistry in the FTC and PTC subtypes. In comparison to the benign cell line, the PTC and FTC cell lines showed an increased peak intensity at 1225 cm^{-1} and 1435 cm^{-1}, and a decreased peak intensity at 1456 cm^{-1} and 1690 cm^{-1}. This indicates an increase in the level of amide III, proteins, and nucleic acids, and a decrease in the amount of lipids and amide I in the cancer cells[40]. The spectral profile of these DTC cell lines show similarities to the characteristic FTC peaks identified in a study by Teixeira *et al.* using thyroid tissue[30]. As both PTC and FTC emanate from epithelial follicular cells and are often even analysed as one group in terms of prognosis, it is plausible that the similarities in their biochemistry observed may be explained by the common origin of PTC and FTC[5,6].

Regarding the UTC cell lines (8505C and C643), both exhibited elevated nucleic acids (~1343 cm^{-1}) and polysaccharides (477 cm^{-1}) in comparison to the benign cell line. A lower peak intensity for amide III was observed for both cell lines in comparison to the benign cell line, which is evident by the broad band in the difference spectrum between ~1190 cm^{-1} and 1280 cm^{-1}. The 8505C cell line showed an increased peak intensity at both 780 cm^{-1} and 830 cm^{-1}, corresponding to increased nucleic acids, which is consistent with the findings of Harris *et al*[23]. The 8505C cell line also showed a higher peak intensity at 1450 cm^{-1} in comparison to the benign cell line, which suggests an increase in the level of proteins and lipids in the cancer cells[40]. UTC is a heterogenous disease at a molecular level, making it difficult to find commonalities between cases, which may explain the dissimilarities in the spectral profiles observed in this study between the two UTC cell lines[42].

The difference spectra of the benign versus the MTC cell lines (MZCRC1 and CRL1803TT) showed consistent spectral bands at 780, 1450, 1570, 1645, and 1673 cm^{-1} that differentiate the MTC cell lines from the benign cell line. In comparison to the benign cell line, the MTC cell lines exhibited a lower peak intensity at 1450 cm^{-1}, indicating lower levels of lipids, carbohydrates and amino acids in

the MTC cells. In comparison to the benign cell line, both MTC cell lines exhibited greater peak intensities at 780 cm^{-1}, 1570 $cm^{-1}$and 1670 cm^{-1}, indicating an increase in the level of nucleic acids (780 cm^{-1}), aspartate and glutamate (1570 cm^{-1}), and amide I (1670 cm^{-1}). As MTCs emanate from the neuroendocrine parafollicular C cells and not from the follicular epithelial cells like the other cell lines, the distinct overlapping spectral features that differentiate the MZCRC1 and CRL1803TT cell lines from the benign cell line may be explained by the distinct origin of MTC[7].

The main focus of this investigation was to evaluate the potential use of Raman spectroscopy as an enhanced diagnostic technique for TC. Objective comparative analysis of the spectra was achieved using linear discriminant analysis (LDA) on already PCA-transformed data sets for maximum class separation. Application of the PC-LDA algorithm to the data achieved diagnostic accuracies up to 99% for the distinction of benign and TC cell lines. The well differentiated PTC and FTC cell lines were detected with sensitivities >90% and specificities >80%, although the model yielded lower performance scores for identifying the UTC cell lines (sensitivities of 77 and 87%, specificities of 73 and 77%, and diagnostic accuracies of 75 and 82% for the 8505C and C643 cell lines, respectively). The heterogeneity and wide variability of molecular profiles of UTCs may explain the poorer performance of the model for discriminating benign cells from individual UTC cell lines as well as the grouped UTC cell lines (diagnostic accuracy of 71%).

A PC-LDA model was applied to examine whether Raman spectroscopy could be used to correctly classify cell lines representing the various subtypes of TC. Diagnostic accuracies from 92%-97% were achieved for the discrimination of the UTC cell lines from FTC and PTC cell lines. The MTC cell lines were discriminated from the PTC, FTC and UTC cell lines with classification model performance scores >93%. The high accuracy observed for the classification of the MTC cell lines may be due to the different origin of MTCs from other TCs, as discussed previously. FTC (XTC1) and PTC (K1) cell lines were discriminated with an accuracy of 87% and the FTC cell line (XTC1) and PTC cell line (TPC1) were discriminated with an accuracy of 85%. Cell lines from the same subtype of TC were then grouped together for analysis. Diagnostic accuracies >81% were achieved for discriminating UTC from the PTC, FTC and MTC subtypes. The model also retained a high level of performance for the discrimination of the MTC subtype from PTC and FTC, with respective diagnostic accuracies of 86 and 99%. The well differentiated PTC and FTC subtypes were then discriminated with a marginally lower diagnostic accuracy of 79%, which may be explained by the common origin of PTC and FTC.

PC-LDA was then applied to investigate the ability to discriminate the benign cells and all the TC subtypes within the same model. The model yielded a poor sensitivity (57%) for the benign cells as benign spectra were misclassified as PTC. Multiple PTC spectra were classified as FTC, resulting in a low diagnostic sensitivity of 63% for PTC. The low discrimination accuracy achieved in this study

between cells derived from the same origin is similar to the findings of Lones *et al*[24]. The MTC and FTC subtypes were discriminated with sensitivities of 100 and 94% respectively, as observed visually in the scatter plot of the linear discriminant scores. The model also yielded a sensitivity of 79% for the UTC subtype. Multiple UTC spectra were misclassified as PTC and benign, as observed in the overlap of the clusters of these subtypes in the scatter plot of the linear discriminant scores.

The benign thyroid cell line could be discriminated from all of the TC subtypes combined into one group with a diagnostic accuracy of 81%. This is slightly higher than the 78.3% reported by Medeiros Neto *et al*.[31], which was achieved applying PC-LDA to Raman spectra obtained from patient thyroid tissue.

The paramount information required from the thyroid FNAC procedure is the differentiation between benign and malignant thyroid nodules. FNAC is the current favoured diagnostic method for the initial investigation of thyroid nodules, with reported sensitivity and specificity ranges of 65%-98% and 78%-100%, respectively[43–46]. The results of this study show that Raman spectroscopy may also be utilized to improve the accuracy of FNAC. In our study, good sensitivities (63%-100%), specificities (65%-100%) and diagnostic accuracies (71%-99%) were achieved for the identification of TC using Raman spectroscopy on TC cell lines prepared as ThinPrep® cytology slides. In conclusion, these data suggests a high potential for using Raman spectroscopy to improve the preoperative diagnosis of TC on FNAC samples; studies are thus warranted to directly test this application.

References

1. Siegel RL, Miller KD, Jemal A. Cancer statistics, 2016. *CA Cancer J Clin*. 2016;66(1):7-30. doi:10.3322/caac.21332.

2. La Vecchia C, Malvezzi M, Bosetti C, et al. Thyroid cancer mortality and incidence: a global overview. *Int J cancer*. 2015;136(9):2187-2195. doi:10.1002/ijc.29251.

3. Davies L, Morris LGT, Haymart M, et al. American Association of Clinical Endocrinologists and American College of Endocrinology Disease State Clinical Review: The Increasing Incidence of Thyroid Cancer. *Endocr Pract*. 2015;21(6):686-696. doi:10.4158/EP14466.DSCR.

4. Lim H, SS D, JA S, Check D, CM K. Trends in thyroid cancer incidence and mortality in the united states, 1974-2013. *JAMA*. 2017;317(13):1338-1348. http://dx.doi.org/10.1001/jama.2017.2719.

5. Gimm O, Dralle H. Differentiated Thyroid Carcinoma. In: Holzheimer R, Mannick J, eds. *Surgical Treatment: Evidence-Based and Problem-Oriented.* Munich: Zuckshwerdt; 2001. https://www.ncbi.nlm.nih.gov/books/NBK6979/.

6. Aboelnaga EM, Ahmed RA. Difference between papillary and follicular thyroid carcinoma outcomes: an experience from Egyptian institution. *Cancer Biol Med*. 2015;12(1):53-59.

doi:10.7497/j.issn.2095-3941.2015.0005.

7. Krysiak R, Marek B, Okopien B. [Medullary thyroid cancer - the present state of art]. *Endokrynol Pol*. 2008;59(5):446-455.

8. Gharib H, Papini E, Paschke R, et al. American Association of Clinical Endocrinologists, Associazione Medici Endocrinologi, and European Thyroid Association medical guidelines for clinical practice for the diagnosis and management of thyroid nodules. *J Endocrinol Invest*. 2010;33(5 Suppl):1-50. doi:10.4158/EP.12.1.63.

9. Bongiovanni M, Spitale A, Faquin WC, Mazzucchelli L, Baloch ZW. The Bethesda System for Reporting Thyroid Cytopathology: a meta-analysis. *Acta Cytol*. 2012;56(4):333-339. doi:10.1159/000339959.

10. Cooper DS, Doherty GM, Haugen BR. Revised American Thyroid Association management guidelines for patients with thyroid nodules and differentiated thyroid cancer. *Thyroid*. 2009;19. doi:10.1089/thy.2009.0110.

11. Hambleton C, Kandil E. Appropriate and accurate diagnosis of thyroid nodules: a review of thyroid fine-needle aspiration. *Int J Clin Exp Med*. 2013;6(6):413-422.

12. Deveci MS, Deveci G, LiVolsi VA, Baloch ZW. Fine-needle aspiration of follicular lesions of the thyroid. Diagnosis and follow-Up. *Cytojournal*. 2006;3:9. doi:10.1186/1742-6413-3-9.

13. Goldstein RE, Netterville JL, Burkey B, Johnson JE. Implications of Follicular Neoplasms, Atypia, and Lesions Suspicious for Malignancy Diagnosed by Fine-Needle Aspiration of Thyroid Nodules. *Ann Surg*. 2002;235(5):656-664.

14. Dutta S, Thaha MA, Smith DM. Do sonographic and cytological features predict malignancy in cytologically indeterminate thyroid nodules? *Ann R Coll Surg Engl*. 2011;93(5):361-364. doi:10.1308/003588411X580160.

15. Sokolov K, Follen M, Richards-Kortum R. Optical spectroscopy for detection of neoplasia. *Curr Opin Chem Biol*. 2002;6(5):651-658. doi:http://dx.doi.org/10.1016/S1367-5931(02)00381-2.

16. Hollas JM. *Modern Spectroscopy*. 4th ed. Chichester: John Wiley & Sons, Ltd.; 2004.

17. Bumbrah GS, Sharma RM. Raman spectroscopy – Basic principle, instrumentation and selected applications for the characterization of drugs of abuse. *Egypt J Forensic Sci*. 2016;6(3):209-215. doi:10.1016/j.ejfs.2015.06.001.

18. Ball DW. Theory of Raman Spectroscopy. *Spectroscopy*. 2001;16(11).

19. Coda S, Siersema PD, Stamp GWH, Thillainayagam A V. Biophotonic endoscopy: a review of clinical research techniques for optical imaging and sensing of early gastrointestinal cancer. *Endosc Int Open*. 2015;3(5):E380-E392. doi:10.1055/s-0034-1392513.

20. Fenn MB, Xanthopoulos P, Pyrgiotakis G, Grobmyer SR, Pardalos PM, Hench LL. Raman Spectroscopy for Clinical Oncology. *Adv Opt Technol*. 2011;2011:1-20. doi:10.1155/2011/213783.

21. Gao P, Han B, Du Y, et al. The Clinical Application of Raman Spectroscopy for Breast Cancer Detection. *Journal of Spectroscopy*. 2017;2017(1).

22. Kong K, Kendall C, Stone N, Notingher I. Raman spectroscopy for medical diagnostics — From in-vitro biofluid assays to in-vivo cancer detection. *Adv Drug Deliv Rev*. 2015;89:121-134.

doi:http://dx.doi.org/10.1016/j.addr.2015.03.009.

23. Harris AT, Garg M, Yang XB, et al. Raman spectroscopy and advanced mathematical modelling in the discrimination of human thyroid cell lines. *Head Neck Oncol*. 2009;1:38. doi:10.1186/1758-3284-1-38.

24. Lones MA, Smith SL, Harris AT, et al. Discriminating normal and cancerous thyroid cell lines using implicit context representation Cartesian genetic programming. In: *IEEE Congress on Evolutionary Computation*. ; 2010:1-6. doi:10.1109/CEC.2010.5586494.

25. Harris AT, Rennie A, Waqar-Uddin H, et al. Raman spectroscopy in head and neck cancer. *Head Neck Oncol*. 2010;2:26. doi:10.1186/1758-3284-2-26.

26. Law AWL, Ahmed R, Cheung TW, Mak CY, Lau C. In situ cellular level Raman spectroscopy of the thyroid. *Biomed Opt Express*. 2017;8(2):670-678. doi:10.1364/BOE.8.000670.

27. Rau J V, Graziani V, Fosca M, et al. Raman spectroscopy imaging improves the diagnosis of papillary thyroid carcinoma. *Sci Rep*. 2016;6:35117. http://dx.doi.org/10.1038/srep35117.

28. Li Z, Li C, Lin D, et al. Surface-enhanced Raman spectroscopy for differentiation between benign and malignant thyroid tissues. *Laser Phys Lett*. 2014;11(4). doi:10.1088/1612-2011/11/4/045602.

29. Rau J V, Fosca M, Graziani V, et al. Proof-of-concept Raman spectroscopy study aimed to differentiate thyroid follicular patterned lesions. *Sci Rep*. 2017;7:14970. doi:10.1038/s41598-017-14872-1.

30. Teixeira CSB, Bitar RA, Martinho HS, et al. Thyroid tissue analysis through Raman spectroscopy. *Analyst*. 2009;134(11):2361-2370. doi:10.1039/B822578H.

31. Medeiros Neto LP, das Chagas E Silva de Carvalho LF, Santos L Dos, et al. Micro-Raman spectroscopic study of thyroid tissues. *Photodiagnosis Photodyn Ther*. 2017;17:164-172. doi:10.1016/j.pdpdt.2016.11.018.

32. A. Téllez Soto C, Neto L, dos Santos L, et al. Infrared and Confocal Raman Spectroscopy to Differentiate Changes in the Protein Secondary Structure in Normal and Abnormal Thyroid Tissues. *Journal of Raman Spectroscopy*. 2017. doi:10.1002/jrs.5370.

33. Desroches J, Jermyn M, Mok K, et al. Characterization of a Raman spectroscopy probe system for intraoperative brain tissue classification. *Biomed Opt Express*. 2015;6(7):2380-2397. doi:10.1364/BOE.6.002380.

34. Ibrahim O, Maguire A, Meade AD, et al. Improved protocols for pre-processing Raman spectra of formalin fixed paraffin preserved tissue sections. *Anal Methods*. 2017;9(32):4709-4717. doi:10.1039/C6AY03308C.

35. Chen D, Plemmons R. *Nonnegativity Constraints in Numerical Analysis*.; 2009. doi:10.1142/9789812836267_0008.

36. Fenn MB, Pappu V. Data Mining for Cancer Biomarkers with Raman Spectroscopy. In: Pardalos PM, Xanthopoulos P, Zervakis M, eds. *Data Mining for Biomarker Discovery*. New York: Springer Science & Business Media; 2012:143-169.

37. Welling M. Fisher linear discriminant analysis. *Dep Comput Sci Univ Toronto*. 2005;3:1-4.

38. Hastie T, Tibshirani R, Friedman J. *The Elements of Statistical Learning*. 2nd ed. New York:

Springer New York; 2009.

39. Šimundić A-M. Measures of Diagnostic Accuracy: Basic Definitions. *EJIFCC*. 2009;19(4):203-211.

40. Movasaghi Z, Rehman S, Rehman IU. Raman Spectroscopy of Biological Tissues. *Appl Spectrosc Rev*. 2007;42(January 2017):493-541. doi:10.1080/05704920701551530.

41. Wreesmann VB, Ghossein RA, Patel SG, et al. Genome-Wide Appraisal of Thyroid Cancer Progression. *Am J Pathol*. 2002;161(5):1549-1556.

42. Kasaian K, Wiseman SM, Walker BA, et al. The genomic and transcriptomic landscape of anaplastic thyroid cancer: implications for therapy. *BMC Cancer*. 2015;15:984. doi:10.1186/s12885-015-1955-9.

43. Gardiner GW, de Souza FM, Carydis B, Seemann C. Fine-needle aspiration biopsy of the thyroid gland: results of a five-year experience and discussion of its clinical limitations. *J Otolaryngol*. 1986;15(3):161-165.

44. Muratli A, Erdogan N, Sevim S, Unal I, Akyuz S. Diagnostic efficacy and importance of fine-needle aspiration cytology of thyroid nodules. *J Cytol*. 2014;31(2):73-78. doi:10.4103/0970-9371.138666.

45. Bagga PK, Mahajan NC. Fine needle aspiration cytology of thyroid swellings: how useful and accurate is it? *Indian J Cancer*. 2010;47(4):437-442. doi:10.4103/0019-509X.73564.

46. Khafagi F, Wright G, Castles H, Perry-Keene D, Mortimer R. Screening for thyroid malignancy: the role of fine-needle biopsy. *Med J Aust*. 1988;149(6):302-303-307.

47. Naumann D. FT-Infrared and FT-Raman Spectroscopy in Biomedical research. In: Gremlich H-U, Yan B, eds. *Infrared and Raman Spectroscopy of Biological Materials*. New York: Marcel Dekker, Inc; 2001:323-379.

Tables

Table 1. Tentative peak assignments for the significant Raman bands identified by spectral variation analysis[40,47].

Wavenumber (cm^{-1})	**Raman peak assignments**
430	Cholesterol ester
454	Ring torsion of phenyl
477	Polysaccharides
509	S-S disulphide stretching band of collagen
524	S-S disulphide stretching in proteins Phosphatidylserine
614	Cholesterol ester
645	C-C twisting mode of phenylalanine
700	Amino acid methionine
729	Adenine
780	Uracil based ring breathing mode
820	Protein band Structural protein modes of tumours Collagen I
855	Proline, tyrosine
880	Tryptophan
941	Skeletal modes of polysaccharides
970	Phosphate monoester groups of phosphorylated proteins and nucleic acids
~1000	Phenylalanine
1100-375	Several bands of moderate intensity belonging to amide III and other proteins
1310	CH3/CH2 twisting or bending mode of lipid/ collagen
1230	Antisymmetric phosphate stretching vibration
1330	Region associated with DNA & phospholipids Collagen
1343	CH3,CH2 wagging (collagen assignment) Glucose CH residual vibrations
1392	C-N stretching, in quinoid ring-benzoid ring-quinoid ring
1402	Bending modes of methyl groups Amino acids aspartic and glutamic acid
1436	CH_2 scissoring

1450	C-H deformation bands (CH functional groups in lipids, amino acids side chains of the proteins and carbohydrates)
1453	Protein bands Structural protein modes of tumors
1499	C=C stretching in benzenoid ring
1570	COO- Aspartate and glutamate
1645	Amide I (α helix)
1650	C=C Amide I Protein amide I absorption
1667	Protein band Carbonyl stretch C=O
1677	Amide I (proteins) C=O stretching (lipids) T, G, C ring breathing modes of DNA/RNA bases

Table 2. Performance of the PC-LDA classification model in discriminating the benign thyroid follicular cell line Nthy-ori 3-1 from each TC cell line.

TC cell line distinguished from Nthy-ori 3-1	**Subtype of TC**	**Sensitivity (%)**	**Specificity (%)**	**Diagnostic accuracy (%)**
XTC1	FTC	100	80	90
K1	PTC	90	87	89
TPC1	PTC	97	87	92
8505C	UTC	77	73	75
C643	UTC	87	77	82
MZCRC1	MTC	100	97	99
CRL-1803TT	MTC	100	93	97

Table 3. Performance of the PC-LDA classification model in discriminating the benign thyroid follicular cell line Nthy-ori 3-1 from TC cell lines grouped by TC subtype.

TC subtype distinguished from Nthy-ori 3-1	Sensitivity (%)	Specficity (%)	Diagnostic accuracy (%)
PTC[†]	85	79	82
UTC[‡]	77	65	71
MTC[§]	84	93	89
DTC[¶]	74	74	74

[†]PTC includes K1 and TPC1. [‡]UTC includes 8505C and C643. [§]MTC includes CRL1803TT and MZCRC1. [¶]DTC includes PTC (K1 and TPC1) and FTC (XTC1).

Table 4. Performance of the PC-LDA classification model in discriminating PTC from UTC cell lines.

Comparison	Sensitivity (%)	Specificity (%)	Diagnostic accuracy (%)
K1 vs. 8505C	93	90	92
K1 vs. C643	93	97	95
TPC1 vs. 8505C	97	93	95
TPC1 vs. C643	93	93	93
PTC[†] vs. UTC[‡]	80	82	81

[†]PTC includes K1 and TPC1, [‡]UTC includes 8505C and C643

Table 5. Performance of the PC-LDA classification model in discriminating MTC from PTC cell lines.

Comparison	Sensitivity (%)	Specificity (%)	Diagnostic accuracy (%)
CRL1803TT vs. K1	100	97	99
MZCRC1 vs. K1	100	93	97
CRL1803TT vs. TPC1	100	100	100
MZCRC1 vs. TPC1	100	100	100
MTC[†] vs. PTC[‡]	90	82	86

[†]MTC includes CRL1803TT and MZCRC1. [‡]PTC includes K1 and TPC1.

Table 6. Performance of PC-LDA classification of FTC lines from PTC, MTC and UTC cell lines.

Comparison	Sensitivity (%)	Specificity (%)	Diagnostic accuracy (%)
XTC1 vs. K1	97	77	87
XTC1 vs. TPC1	89	80	85
XTC1 vs. 8505C	100	87	94
XTC1 vs. C643	97	97	97
XTC1 vs. CRL1803TT	100	100	100
XTC1 vs. MZCRC1	100	100	100
FTC[†] vs. PTC[‡]	89	69	79
FTC[†] vs. MTC[§]	100	98	99
FTC[†] vs. UTC[¶]	97	81	89

[†]FTC includes XTC1. [‡]PTC includes K1 and TPC1. [§]MTC includes CRL1803TT and MZCRC1. [¶]UTC includes 8505C and C643.

Table 7. Performance of the PC-LDA classification model for discriminating the MTC from UTC cell lines.

Comparison	Sensitivity (%)	Specificity (%)	Diagnostic accuracy (%)
CRG1803TT vs. 8505C	100	93	97
MZCRC1 vs. 8505C	100	97	99
CRG1803TT vs. C643	96	97	97
MZCRC1 vs. C643	100	100	100
MTC[†] vs. UTC[‡]	78	90	84

[†]MTC includes CRL1803TT and MZCRC1. [‡]UTC includes 8505C and C643.

Table 8. Performance of the PC-LDA classification model for discriminating the benign and TC subtypes.

Comparison	Sensitivity (%)	Specificity (%)
Benign	57	98
FTC[†]	94	92
PTC[‡]	63	91
UTC[¶]	79	96
MTC[§]	100	96

[†]FTC includes XTC1. [‡]PTC includes K1 and TPC1. [¶]UTC includes 8505C and C643. [§]MTC includes CRL1803TT and MZCRC1.

Table 9. Performance of the PC-LDA classification model for discriminating the benign cell line from all TC lines.

Comparison	Sensitivity (%)	Specificity (%)	Diagnostic accuracy (%)
Benign vs TC[†]	74	87	81

[†]TC includes representative spectra from FTC, PTC, UTC, and MTC.

Figure legends

Figure 1. Mean Raman spectrum of the benign cell line (NThy-ori 3-1) with the standard deviation shown as shading, and the different spectral regions with corresponding biomolecules.

Figure 2. Difference spectrum between **(a)** Nthy-ori 3-1 (benign) and FTC cell line XTC1; **(b)** Nthy-ori 3-1 and PTC cell line K1; **(c)** Nthy-ori 3-1 and PTC cell line TPC1. Shading indicates regions of the spectrum that were significantly different ($p<0.05$).

Figure 3. Difference spectrum between **(a)** Nthy-ori 3-1 (benign) and 8505C (UTC); and **(b)** Nthy-ori 3-1 and C643 (UTC). Shading indicates regions of the spectrum that were significantly different ($p<0.05$).

Figure 4. Difference spectrum between **(a)** Nthy-ori 3-1 (benign) and CRL1803TT (MTC); **(b)** Nthy-ori 3-1 and MZCRC1 (MTC). Shading indicates regions of the spectrum that were significantly different ($p<0.05$).

Figure 5. Scatter plot of the linear discriminant scores of the benign spectra and representative spectra from each TC subtype using PC-LDA.

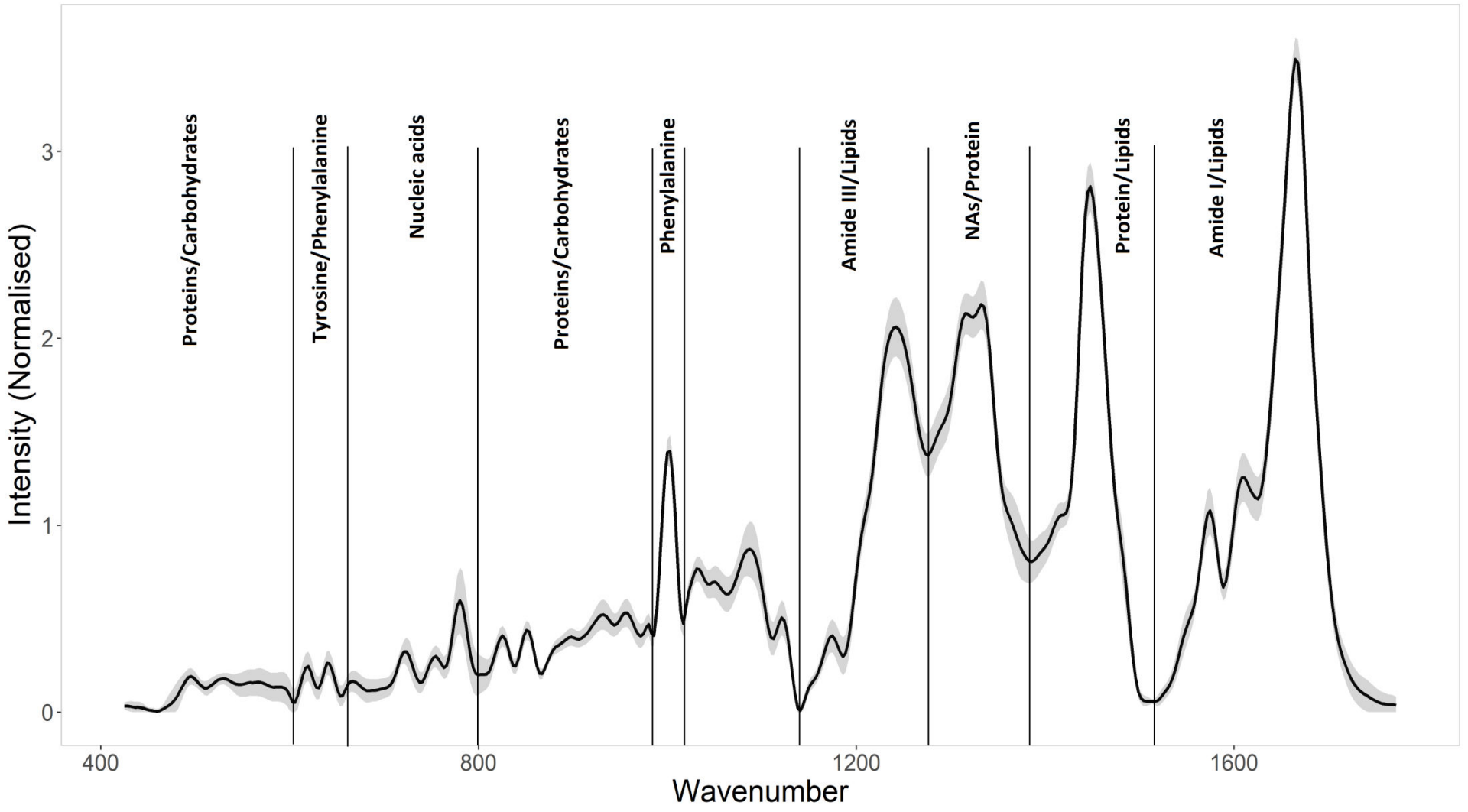
Proteins/Carbohydrates
Tyrosine/Phenylalanine
Nucleic acids
Proteins/Carbohydrates
Phenylalanine
Amide III/Lipids
NAs/Protein
Protein/Lipids
Amide I/Lipids
Intensity (Normalised)
0
1
2
3
400
800
1200
1600
Wavenumber

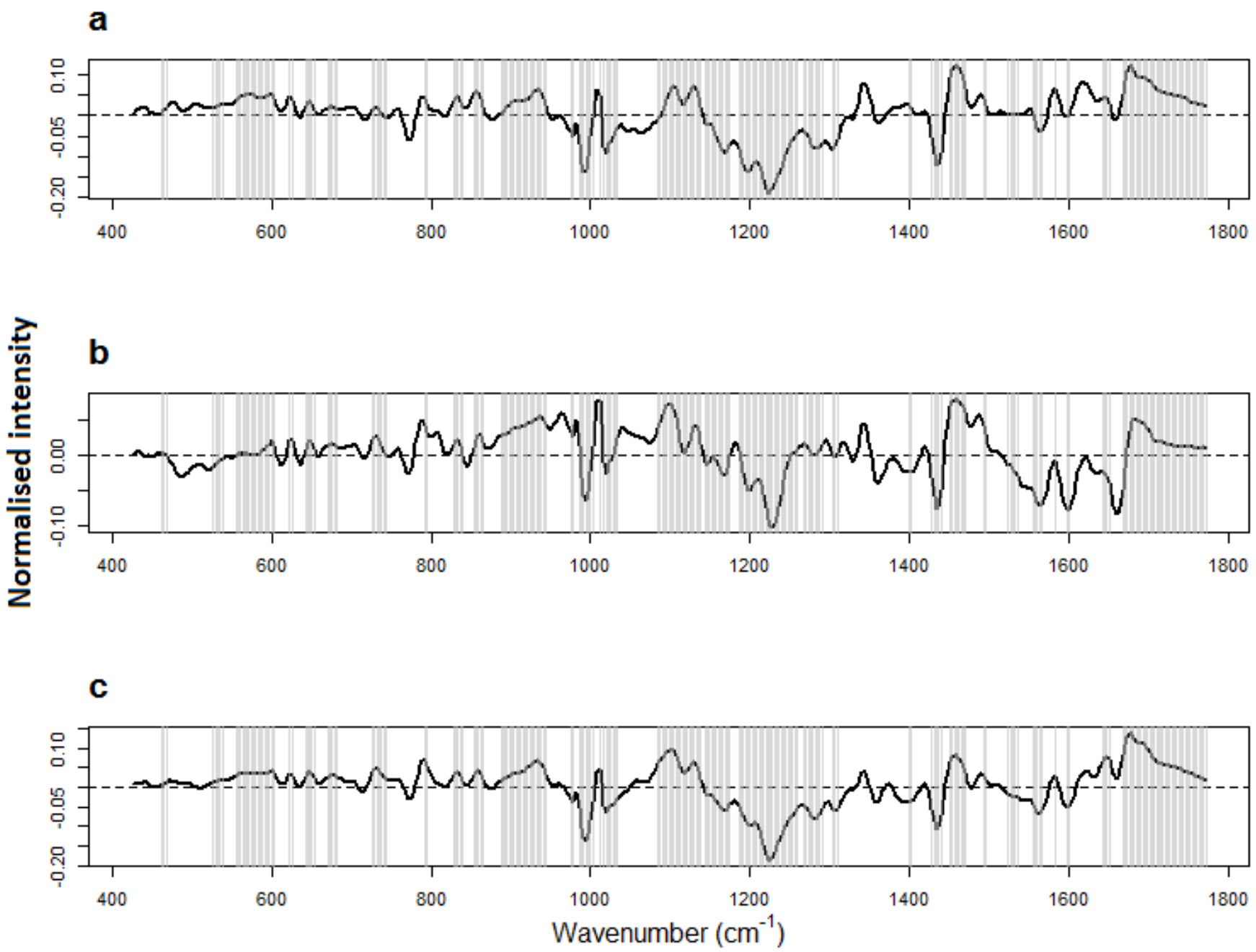
a
b
c
Normalised intensity
0.10
-0.05
-0.20
0.00
-0.10
400
600
800
1000
1200
1400
1600
1800
Wavenumber (cm-1)

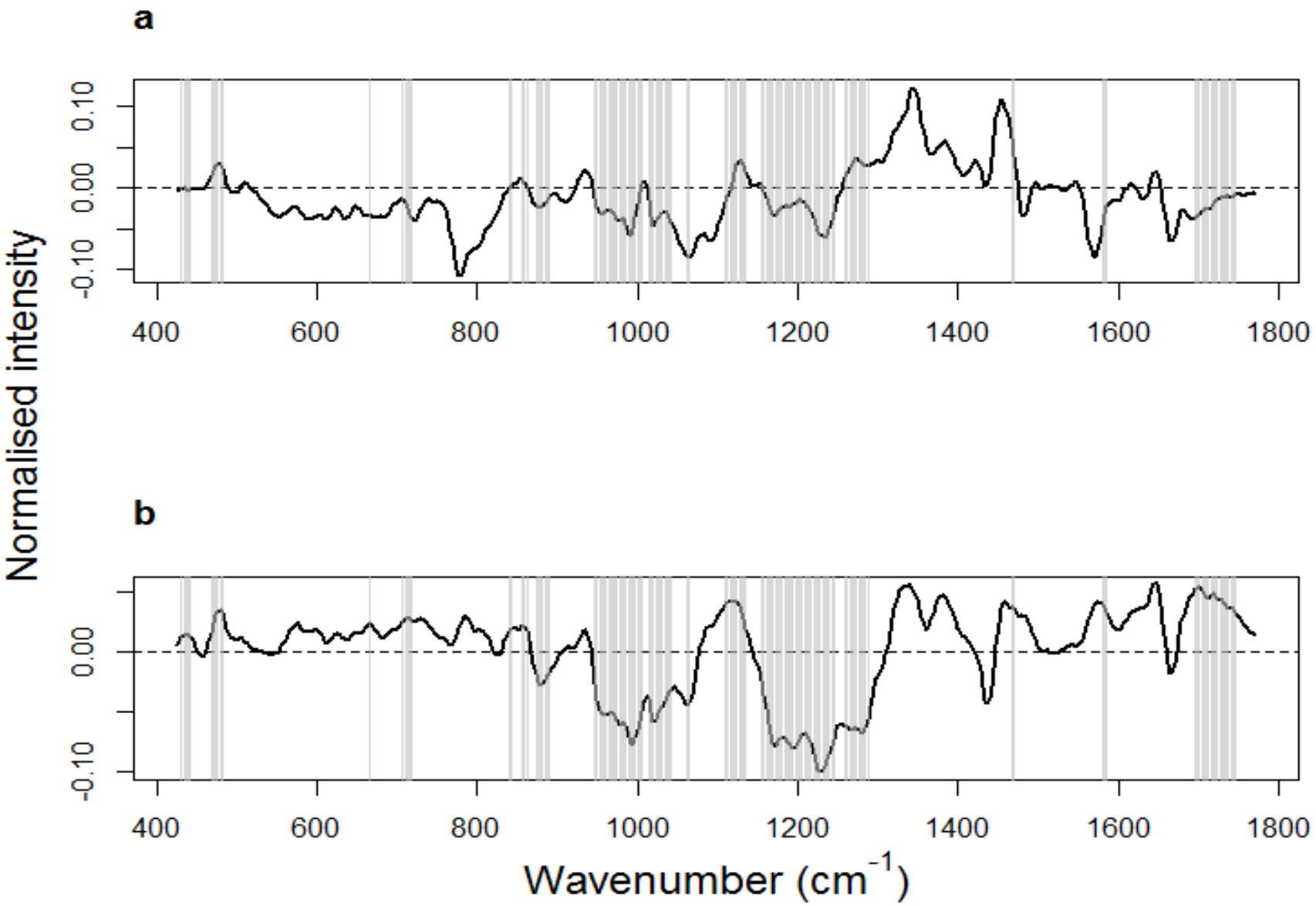
a
b
Normalised intensity
0.10
0.00
-0.10
400
600
800
1000
1200
1400
1600
1800
Wavenumber (cm^{-1})

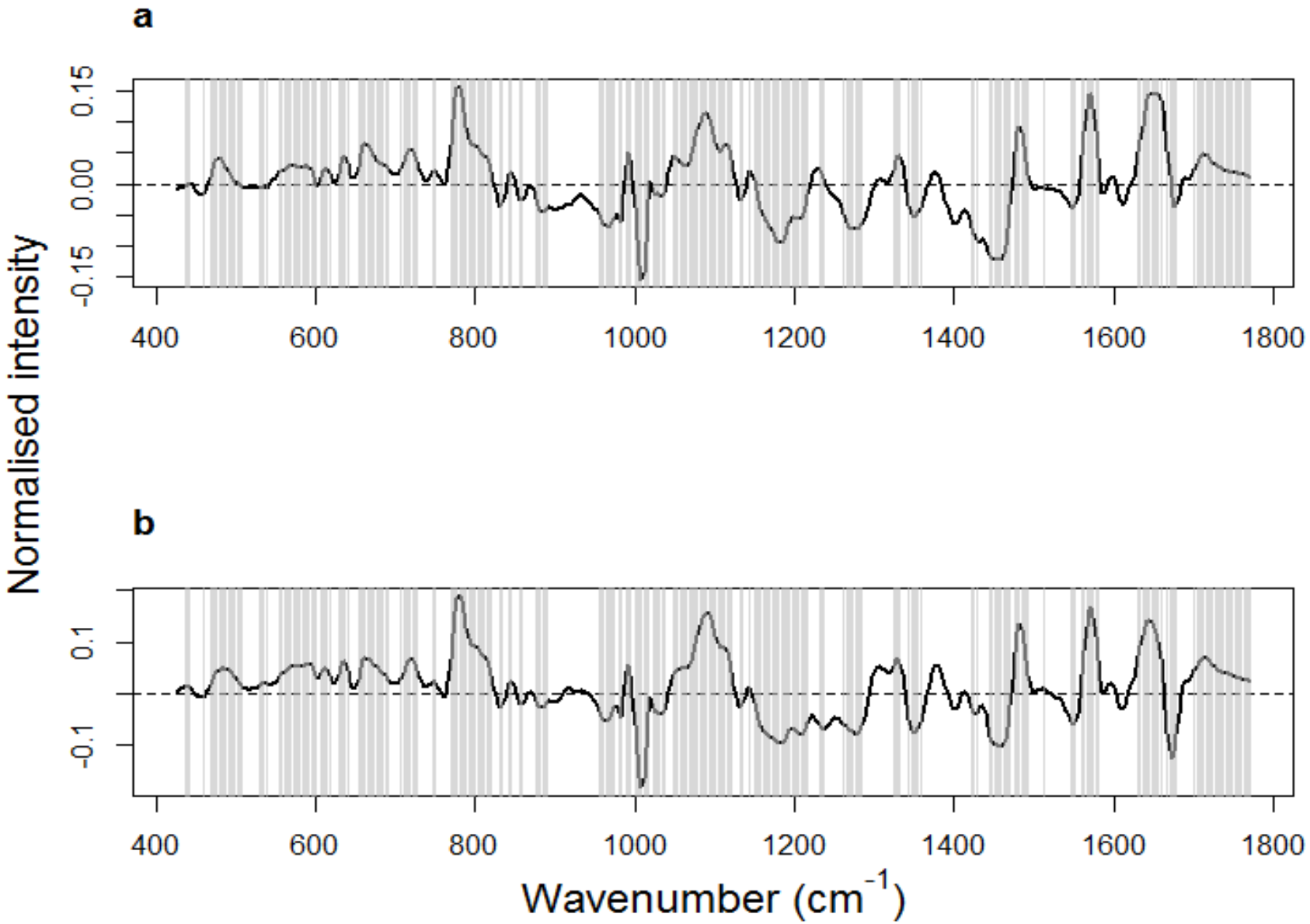
a
b
Normalised intensity
0.15
0.00
-0.15
0.1
-0.1
400
600
800
1000
1200
1400
1600
1800
Wavenumber (cm-1)

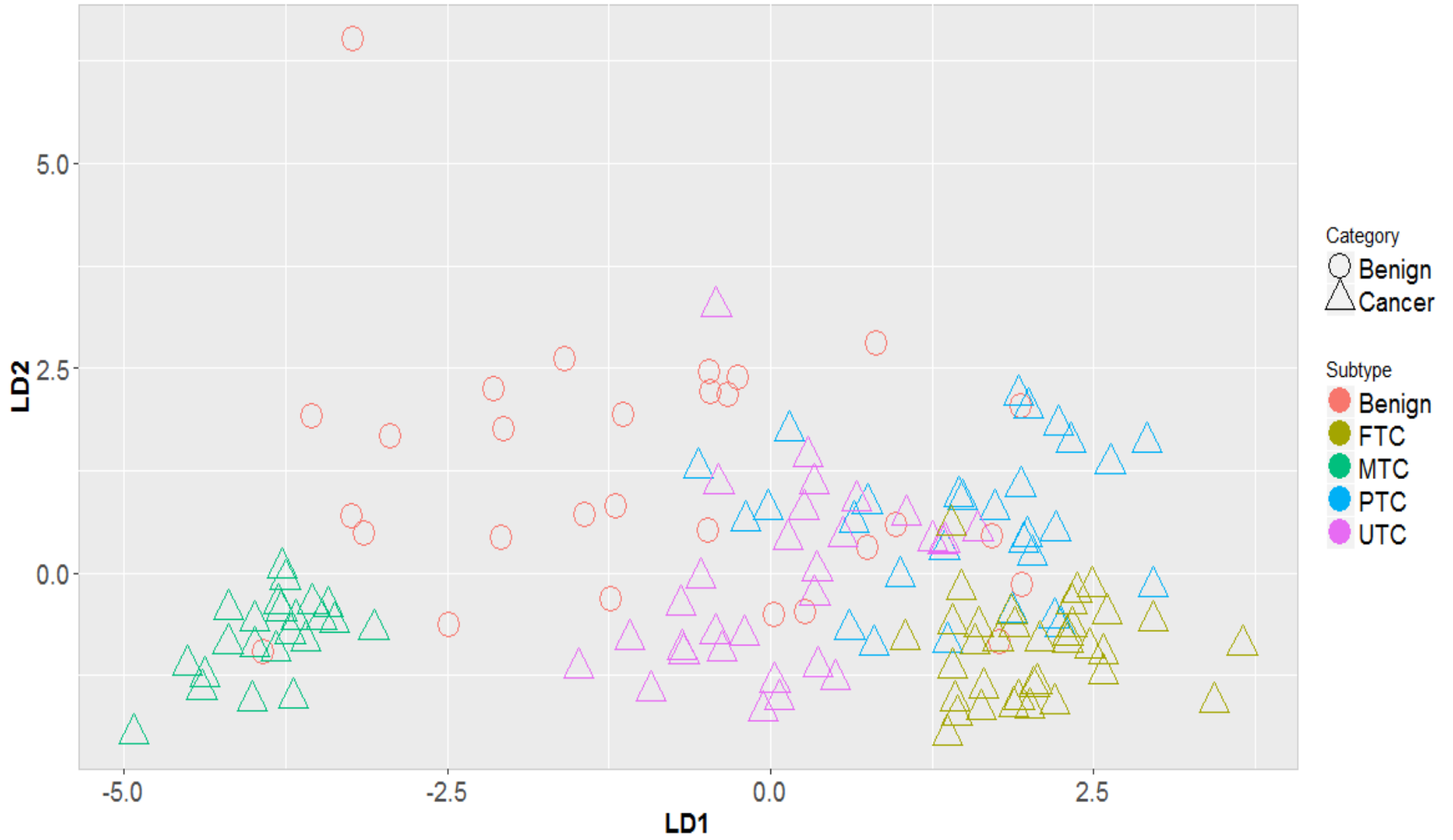
5.0
2.5
0.0
LD2
-5.0
-2.5
0.0
2.5
LD1
Category
Benign
Cancer
Subtype
Benign
FTC
MTC
PTC
UTC